

INVESTIGATION OF CONCRETE FILLED COMPOSITE PLATE SHEAR WALLS USING FINITE ELEMENT METHODS

Erkan POLAT * 

Received: 17.09.2019; revised: 06.01.2020; accepted: 09.01.2020

Abstract: Concrete filled composite plate shear wall is an innovative structural lateral force resisting system that is being investigated experimentally and numerically. It consists of pre-fabricated steel web plates that are spaced parallel to each other by having regularly spaced cross-connecting tie bars (rods) which is then filled with concrete. This paper make use of previously developed numerical models and extends the study to investigate different aspects of wall behavior. In this study, two of the previously tested wall models were used to investigate percentage of steel plate yielding at certain wall elevations per certain drift levels, steel plate von-Mises stress contours, the distribution of cracks in concrete, relative contribution of steel plates and concrete to total wall base shear and axial stress distribution of steel plate and concrete. The study assumes fixed-based walls and describes the development of finite element models using LS-Dyna.

Keywords: Steel-concrete composite structures, seismic, finite element, modeling

Beton Dolgu Kompozit Levha Perde Duvarların Sonlu Elemanlar Metodu Kullanılarak İncelenmesi

Öz: Beton dolgu kompozit levha perde duvar, deneysel ve sayısal olarak araştırılan yenilikçi bir yapısal yanal kuvvet direnç sistemidir. Önceden imal edilmiş çelik levhaların birbirine paralel yerleştirilerek bağlantı çubukları ile bağlanması ve levhalar arasındaki boşluğun beton ile doldurulması ile meydana gelir. Bu makalede, daha önce geliştirilmiş sayısal modellerden yararlanılmakta ve duvar davranışının farklı yönlerini araştırmak için çalışmayı genişletmektedir. Bu çalışmada, daha önce test edilmiş iki duvar modeli kullanılarak; belli duvar yüksekliğindeki çelik levhaların belli ötelenme oranına göre akma oranı, çelik levha von-Mises gerilme dağılımları, çatlakların beton üzerindeki dağılımları, çelik levha ve betonun toplam duvar taban kesme kuvvetleri üzerindeki oransal katkıları ve çelik levha ve betonun eksenel gerilme dağılımları incelenmiştir. Çalışmada, sabit mesnetli duvarlar varsayılmakta ve sonlu eleman modellerinin LS-Dyna kullanılarak oluşturulması açıklanmaktadır.

Anahtar Kelimeler: Çelik-beton kompozit yapılar, sismik, sonlu elemanlar, modelleme

1. INTRODUCTION

Concrete plate shear wall–concrete filled (C-PSW/CF) is composed of pre-fabricated structural steel plates assembled by having regularly spaced cross-connecting tie bars (rods) which is then filled with concrete (AISC 2016). The steel plates serve as a formwork for the concrete while it is casting and serve as reinforcement after casting. The cross-connecting tie bars (either welded or bolted to steel plates) are used to: help erect the empty wall modules; transfer axial, shear and moment at steel-concrete interface, and; reduce local buckling length of the steel plates. (In some cases, shear studs can also be used together with the tie bars and different country codes might permit different connectors in addition to tie bars and shear studs;

* Department of Civil Engineering, Munzur University, Tunceli 62000, Turkey.
İletişim Yazarı: Erkan POLAT (erkanpolat@munzur.edu.tr)

i.e., beaten connector, T-shape connector or combination of connectors). C-PSW/CF allows modular construction and reduce construction time and cost. Issues encountered in the construction of conventional reinforced concrete shear walls, such as rebar congestion due to need of large volume of reinforcement at the wall base, are eliminated. For C-PSW/CF, reinforcement ratio is given simply the area of the steel plates to area of the infill concrete. Other advantages of these wall systems are, smaller footprints than conventional reinforced concrete walls, speed in construction owing to reduced labor and on-site work.

C-PSW/CF is used as a lateral force resisting system in buildings. Based on the wall aspect ratio, (ratio of wall height to section length) the wall is classified as flexural or shear type. A Wall having an aspect ratio larger than one is classified as flexural type. In this study flexural type wall is considered. AISC (2016) permits C-PSW/CF to have circular or half-circular concrete filled tubes as boundary elements. Flexural type C-PSW/CF is expected to develop plastic moment capacity at the wall base which assumes fully yielded steel plate, and concrete that attained unconfined compressive strength. Energy dissipation is mainly achieved by axial yielding of the steel plates at the wall base such that the wall develops plastic hinge at the base. Past experimental and numerical studies on flexural type walls indicated good seismic performance such as high stiffness, strength and displacement ductility (Alzeni and Bruneau 2017; Eom et al. 2009). Steel plate concrete composite walls have been studied by many researchers; (Wright et al. 1991); Wright et al. (1991), Eom et al. (2009); Ramesh (2013); Alzeni and Bruneau (2017); Polat and Bruneau (2017). These type of wall systems have been used in some high-rise buildings, including Rainer Square Tower in Seattle, China World Trade Center.

In this study a previously tested two C-PSW/CF are under review. These walls have boundary elements of circular and half-circular HSS. The paper first describes the physical properties of the walls and then introduces the finite element modeling phases (material models, element models, contact model etc.). The following aspects of wall behavior are investigated: percentage of steel plate yielding at certain wall elevations per certain drift levels, steel plate von-Mises stress contours, the distribution of cracks in concrete, relative contribution of steel plates and concrete to total wall base shear and axial stress distribution of steel plate and concrete. The study is expected to contribute to the existing knowledge of these wall systems.

2. DESCRIPTION OF WALL MODELS

Two flexural types C-PSW/CF were considered in this study. These walls were previously tested for their cyclic inelastic response by Alzeni and Bruneau (2017) and numerically studied by Polat and Bruneau (2017). **Figure 1** shows the cross-section of the wall models. The wall shown in **Figure 1(a)** was denoted as B1 and consisted of round HSS columns at the wall boundaries and dual web plates in between. The wall shown in **Figure 1(b)** was denoted as NB1 and consisted of half round HSS as boundary elements. Walls B1 and NB1 have a web plate width, b , of 30 in. and 40 in., concrete thickness, t_c , of 6 in. and 8 in., respectively. Both walls have a steel plate thickness, t , of 5/16 in. Regularly spaced cross tie bars were used to connect web plates. The diameter of the tie bars is 1 in. and the tie spacing, S , is equal in horizontal and vertical direction and equal to 8 in. The total cross-section depth of the walls, W , are 44 in. and 48.625 in., for B1 and NB1, respectively. The walls are cantilever type and have a total height of 120 in. from the base.

Figure 1 shows the steel and concrete axial stress distribution, and compression depth C , assumed in the calculation of wall plastic moment (flexural type walls resist lateral load by developing plastic hinge and plastic moment at the wall base). The stress distributions are uniform, where F_y is the yield strength of the steel skin, and f'_c is the compressive strength of the concrete. Alzeni and Bruneau (2014) provided closed form equations for analytical calculation of wall plastic moments.

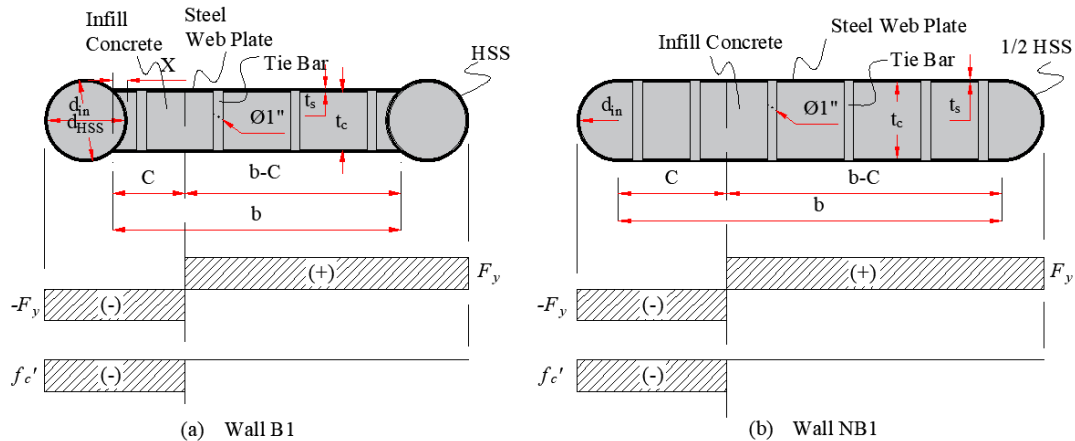


Figure 1:
Concrete filled composite plate shear wall (C-PSW/CF) models

3. FINITE ELEMENT MODELING

Finite element modeling of the walls was previously developed by Polat and Bruneau (2017) using LS-Dyna. A summary of the modeling methods is presented herein. LS-Dyna is a general-purpose finite element program and allows stress analysis of structures under various loading conditions. It was recognized that the wall models shown in **Figure 1**, were symmetric for a plane located at the center parallel to the axis of loading. Therefore, symmetry conditions could be used in finite element modeling to save time in the analysis part of the study considering the highly nonlinear nature of the simulation. **Figure 2** shows the finite element model developed for Model B1 in LS-Dyna. Solid element was used to model concrete; shell element was used to model steel plates and beam element was used to model tie bars. Fixed boundary conditions were defined at the wall base. Displacement conditions were defined for the top nodes of the steel and concrete elements. The cyclic displacement curve definition in LS-Dyna was provided by Polat and Bruneau (2018).

3.1. Steel Material Model

A bilinear material model was considered to model the material behavior of the steel web plates, HSS and tie bars in the numerical model. In LS-Dyna this was achieved by using *mat_plastic_kinematic* (Mat003) (LSTC 2013) model. **Figure 3** illustrates the schematic of this material model for elastic modulus, E , yield stress, F_y , tangent modulus, E_t , and hardening parameter β ($\beta=0$ corresponds to kinematic hardening, and $\beta=1$ to isotropic hardening). For Model B1, $E=29000$ ksi, $E_t=100$ ksi, $F_y=62$ ksi for the web plate, and, $E=27500$ ksi, $E_t=80$ ksi, $F_y=56$ ksi for the HSS. For Model NB1, $E=29000$ ksi, $E_t=80$ ksi, $F_y=61$ ksi for the web plate, and $E=27500$ ksi, $E_t=50$ ksi, $F_y=52$ ksi for the HSS.

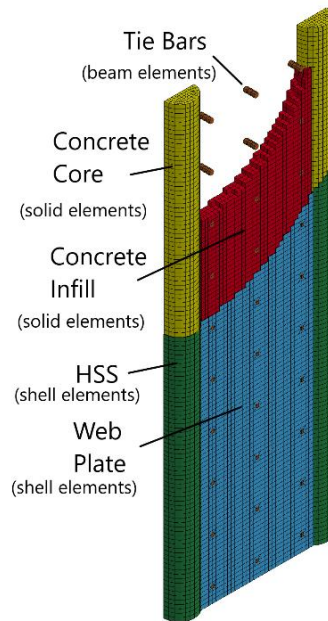


Figure 2:
Finite element model developed in LS-Dyna

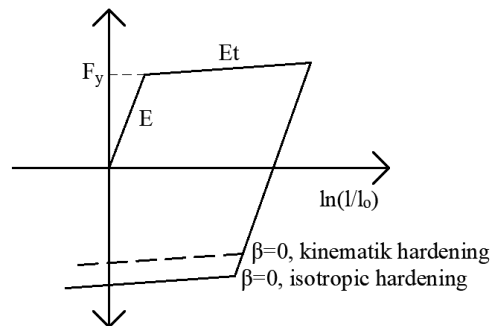


Figure 3:
Schematic of stress strain behavior of Mat003 of LS-Dyna

3.2. Concrete Material Model

The Winfrith (Mat085) (LSTC 2013) material model was considered to model the concrete parts of the wall models. This material model is based on the work of Broadhouse and Neilson (1987) and Broadhouse (1995). This material model requires little input and popular among structural modeling of concrete for various loading conditions. The most important feature of this material model is that it allows crack planes in three directions per element and the crack formation can be reviewed by post-processing. The material parameters that are needed to be defined are: Tangent modulus; Poisson’s ratio; uniaxial compressive strength; uniaxial tensile strength; crack width (if strain rate=0, otherwise fracture energy should be used), and; aggregate size. The crack formulation used in the Winfrith Concrete Model is based on Wittmann et al. (1988) and it considers, aggregate size, concrete compressive strengths, loading rates, water-to-cement ratios, and test specimen size (Schwer 2011). The compression strength of concrete was about 7 ksi for both walls and the tangent modulus was taken equal to 2400 ksi.

The walls were tested under quasi static displacement (dynamic effects were negligible). In the numerical model the strain rate effect was, therefore, zero, and crack width (at which the crack-normal tensile stress goes to zero) was used as an input for Winfrith concrete. The crack opening width for the zero tensile stress (w) can be calculated from: $w = 2G_F/f_t$, where G_F is the fracture energy and f_t is the tensile strength of the concrete (f_t was assumed equal to 10% of the concrete compressive strength). The fracture energies for the selected aggregate size was taken from Table 2.1.4 from Clark (1995) for a particular concrete compressive strength and maximum aggregate size. For the work presented here, the maximum aggregate size was selected as 0.31in. (8 mm). The corresponding fracture energy for 7 ksi is 85Nm/m². The corresponding crack width was calculated to be as 0.0014in. (0.035) and 0.0016in. (0.039mm).

3.3. Contact between Steel Skin and Infill Concrete

A contact definition is needed to simulate the interaction and relative sliding of the wall segments (steel and concrete). Sliding surfaces can be treated in LS-Dyna in several ways. The penalty method (Hallquist 2006) is the most preferred contact method and was considered in the contact definition for the wall simulations. **Figure 4** illustrates the penalty method implementation in the LS-Dyna contact model. The contact algorithm first defines the sliding surfaces in contact as slave side and master side and identifies the nodes as master nodes (nodes lying on master surface), and slave nodes (nodes lying on the slave surface). In this method, each slave node is checked for penetration through the master surface. When penetration occurs, a force proportional to the amount of penetration is applied between the slave node and the master segment. The penetration of nodes and the resulting reaction force can be visualized with a hypothetical interface spring as illustrated in **Figure 4**.

The contact force, F_i , is a function of node penetration and spring stiffness: $F_i = \delta_i k$. where δ_i is the amount of penetration of each node and k is the interface spring stiffness; for solid elements: $k = fKA^2/V$; for shell elements: $k = fKA/\max(\text{shell diagonal})$, where K is the bulk modulus, f is penalty factor, V is the element volume, and A is the face area of the element. It is reported that (Hallquist 2006) the contact may fail if the default stiffness is very small. In the standard penalty formulation, the default interface stiffness is taken as the minimum of the master segment and slave node stiffness. If the interface stiffness is very low, a contact failure can occur; to account for this, interface stiffness can be scaled, but very large values may cause instability problems (Hallquist 2006). In the simulations, the interaction between the segments of the wall was defined using the *automatic_surface_to_surface_mortar* contact model with static interface friction coefficient of 0.3. Studies by Polat and Bruneau (2017) showed that the default interface stiffness values were low causing slippage between the wall segments, therefore an increased contact stiffness was used.

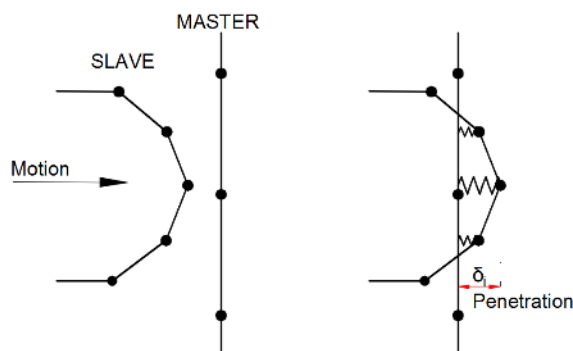


Figure 4:
Illustration of penalty method in LS-Dyna

3.4. Mesh Size Convergence Study

The final mesh size of the concrete and steel plates were selected based on the results of a mesh convergence study as briefly explained here. In the first mesh considered, the infill concrete was modeled using 1.0 x 1.0 x 1.0 in. solid elements and the plates were modeled using 1.0 x 1.0 in. shell elements. This mesh size is referred here as Mesh 1. In the second mesh considered, shell and solid element sizes were reduced in half, resulting in 0.5 x 0.5 x 0.5 in. solids element and 0.5 x 0.5 in. shell elements. This mesh size is referred here as Mesh 2. Wall responses from the two cases were obtained under cyclic loading and compared. **Figure 5** shows the comparison of cyclic wall response based on element mesh sizes. Results implied that with reduced mesh sizes the wall response keeps identical, therefore, the use of element sizes based on Mesh 1 was deemed to be adequate.

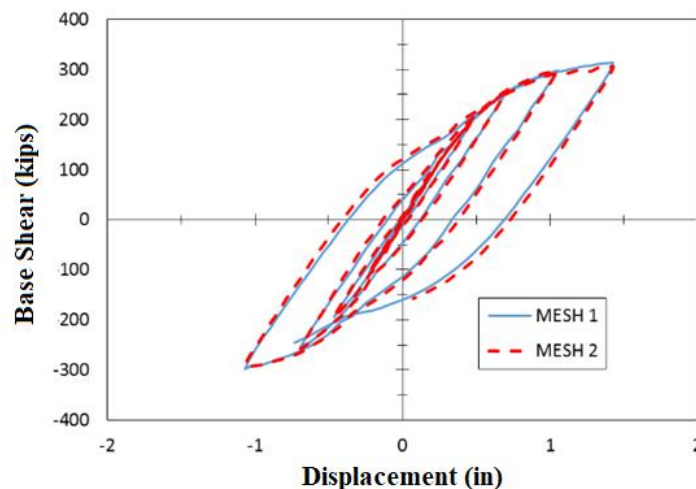


Figure 5:
Comparison of cyclic wall response based on element mesh sizes

4. PERCENTAGE OF STEEL PLATE YIELDING

In this section, amount of steel plate yielding of the wall models at certain wall elevations and drift levels is investigated. For C-PSW/CF, flexural bending results in large axial strains at the wall base and locations away from the wall neutral axis. For this reason, yielding of the steel plates is initiated, first, at wall base and outermost fibers of the cross-section until plastic hinge is fully developed. The strain at which the steel plates start yielding can be calculated from $\epsilon_y = F_y/E_s$. The yielding strain can then be compared against the numerically obtained strain values to determine the amount of yielding. In numerical models, axial strain values were obtained as the average of the three integration points used across the thickness of the shell elements. At randomly selected wall elevations of 3 in., 10 in., 16 in., 24 in., 32 in., and 40 in. average axial strain values were determined for every shell element. Then, at certain wall drift levels, numerically obtained strain values were compared with the yield strain to determine the amount of yielding of the steel plates for a given wall elevation.

Figure 6 and **Figure 7** show the amount of steel plate yielding (as percentage of the total steel area of the cross-section) for the specified wall elevations and drift levels for Model B1 and NB1, respectively. It is seen from the figures that, for both wall models, yielding started after about 0.2% drift ratio; before that the entire section was elastic. For Model B1 (**Figure 6**), the amount of yielding reached 100% only at 3 in. elevation out of the other specified elevations. For higher elevations yielding amount was below 100%. At 3 in. elevation, entire section was yielded at about 2.0% drift ratio. At this drift ratio, the amount of steel plate

yielding for the 10 in., 16 in., 24 in., 32 in., and 40 in. wall elevations were 83%, 46%, 35%, 21% and 10%, respectively. It should be noted that the total cross-section depth of Model B1 is 44 in. which may be taken as plastic hinge length. Above results indicate that steel plates would likely to remain elastic above this value. Similarly, as shown in **Figure 7** for Model NB1, the entire steel section was yielded at 3 in. elevation after reaching 1.8% drift ratio. At this drift ratio, the amount of steel plate yielding for the 10 in., 16 in., 24 in., 32 in., and 40 in. wall elevations were 94%, 50%, 31%, 23% and 13%, respectively. Recalling that the total cross-section depth of Model B1 is 48.6 in., and at 40 in. elevation 13% of the steel section was yielded, it would be reasonable to assume that for Model NB1 the plastic hinge length is equal to total cross-section depth. It should be noted that, the numerical model of B1 attained plastic moment value at the base between the drift ratios of 0.44% and 0.67%. The numerical model of NB1 attained the specimen plastic moment capacity at the base between the drift ratios of 0.60% and 0.90%.

5. VON-MISES STRESS CONTOURS AND CONCRETE CRACK DISTRIBUTION

In the previous section the amount of steel plate yielding was quantitatively and graphically presented for certain wall elevations close to wall base and at different wall drifts. Here formation of steel plate yielding is presented in terms of yield stress contours for the entire wall elevation. For the steel material considered in the numerical simulation, yielding is based on von-Mises criterion. Such that the theoretical uniaxial yield strain (or stress) considered in the previous section might be less or high due to interaction of shear, tensile and compressive stresses on the steel plate (however, it is little significance for the purpose of this section). **Figure 8** and **Figure 9** show the von-Mises stress contours at different drift levels for Model B1 and NB1, respectively. In these figures maximum stress was set equal to 62 ksi and the element stresses that reached this value is shown with red color. As seen from these figures, plate elements were slightly yielded at about at 0.4% drift ratio and entirely yielded at about 2.0% drift ratio at the wall base. The von-Mises yield stress contours indicate also the formation of plastic hinge at high drift ratios (i.e. 2%). The plastic hinge length can be seen to equal approximately to wall depth.

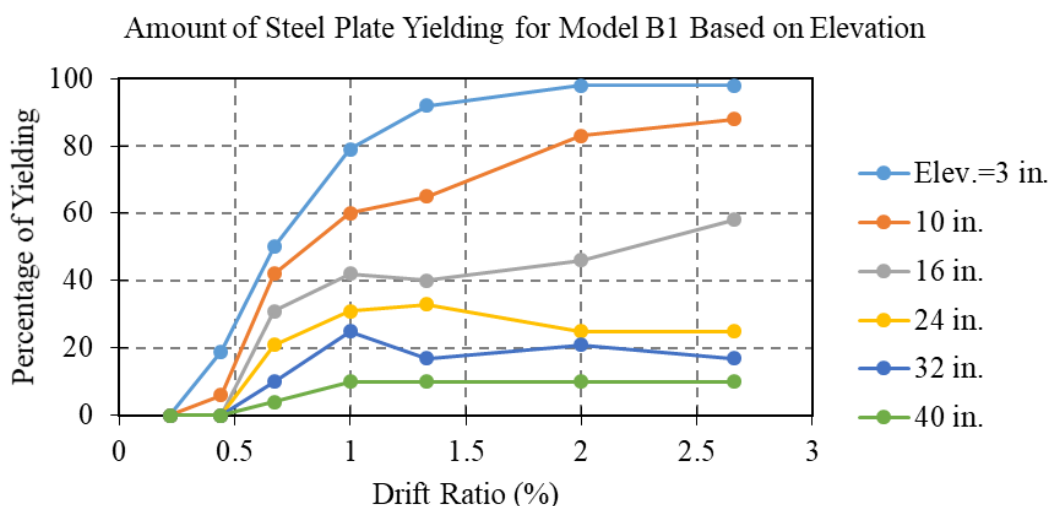


Figure 6:
Amount of steel plate yielding of Model B1 at specified wall elevations and drifts

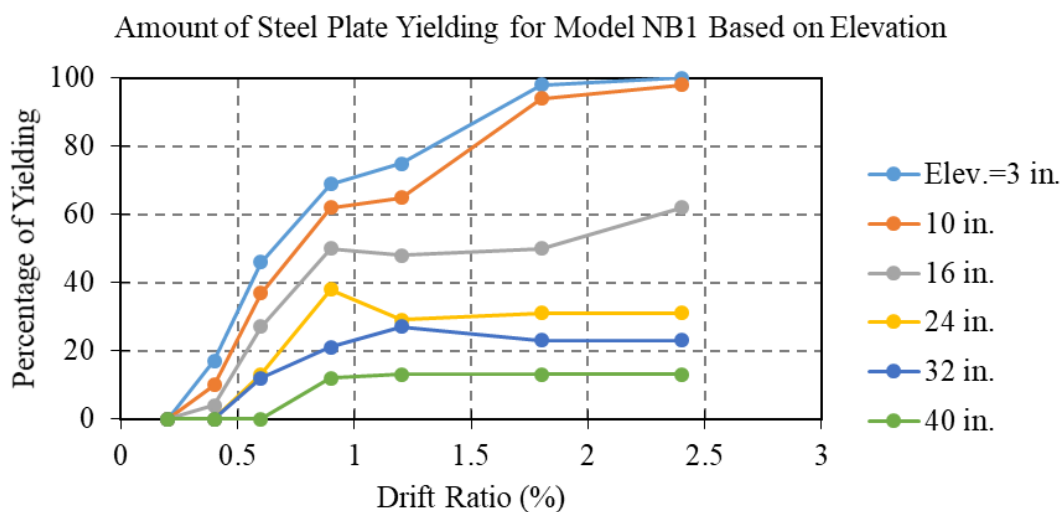


Figure 7:
Amount of steel plate yielding of Model NB1 at specified wall elevations and drifts

Figure 10 and **Figure 11** show the formation of concrete cracking along the height of the wall models, for B1 and NB1, respectively. The crack formations are reported at wall drift ratios of 0.6%, 0.9%, 1.2% and 1.8% for B1, and; 0.67%, 1.0%, 1.33% and 2.0% for NB1. The direction of the cracks (on the tension side of the wall) is horizontal to surface and consistent with the flexural behavior of the wall. Note that, compressive cracks, formed vertically on compression side of the wall, are also visible (i.e., at 2% in **Figure 10** and 1.8% in **Figure 11**). Cracks are more concentrated at the wall base where plastic hinging develops. The lengths of the cracks increase with increasing wall deformation. At the wall base crack lengths extends as far as to the location of plastic neutral axis of the wall. Under increasing wall deformation, crack sizes increase both in number and size. It should be noted that the location of the cracks along the wall height coincides with the vertical location of the row of tie bars used along the wall height (i.e., cracks were formed at a certain spacing which was equal to tie spacing). This behavior shows that tensile forces are transferred by tie bars to infill concrete (noting that concrete starts cracking at little tensile stresses which explains the flexural crack formation at tie locations). It should also be noted from **Figure 10** that, for the concrete core (within the HSS) of Model B1, the crack distribution is more uniform than the infill concrete within the wall web. This is because no tie bars were used within the HSS part of the wall, and the cracking was a result of interface friction created by surface pressure between concrete core and HSS.

6. CONTRIBUTION OF STEEL AND CONCRETE TO TOTAL SHEAR FORCE

In flexural type C-PSW/CF, the steel skin carries tensile and compressive stresses, and the concrete carries mostly compressive stresses and negligible tensile stresses. The moment resistance of each part is calculated from the tension and compression force vectors resulting from the tensile and compressive axial stresses of the wall parts. The shear resistance of each component can analytically be calculated as the ratio of base moment they resist to total wall height. For the numerical study, the shear force resistance of each wall component can be obtained by extracting shear stresses for steel and concrete for certain elevation of wall cross-section and having the shear stresses integrated across the component cross-section.

Using the analysis results, shear forces from concrete and steel parts of the wall were extracted separately at regular spacing along the wall height. **Figure 12(a-b)** shows the relative contribution of the steel and concrete to total base shear resistance of the wall models B1 and

NB1, respectively. The relative shear contribution of wall parts along the wall height is more uniform for Model B1 than Model NB1. For Model B1, the relative contribution of concrete **Figure 12(a)** was gradually reduced with increasing wall drift. The largest reduction in shear resistance of concrete occurs at about 20 in. wall elevation which is within the region of wall plastic hinge length. The gradual reduction in shear resistance of concrete was a result of concrete cracking which was increased in size and number with wall drift (as demonstrated in the previous section). Similarly, for Model NB1, the relative contribution of concrete **Figure 12(b)** was reduced with increasing wall drift. However, the pattern of reduction was not as uniform as compared to that of Model B1. **Figure 12(b)** shows that, following 1.2% drift ratio, the shear contribution of concrete increases at about 20in. wall elevation while opposite is true for the steel. This behavior was a result of development of local plate buckling of the steel web plate (more significant in Model NB1 than B1) which becomes significant under larger drift levels. Following local buckling, the steel plate loses some of the shear force resistance to concrete. The same behavior was not observed for Model B1 which is attributed to presence of full HSS used for that wall. In the following section, the influence of local plate buckling on wall base axial stresses will be investigated for both wall models.

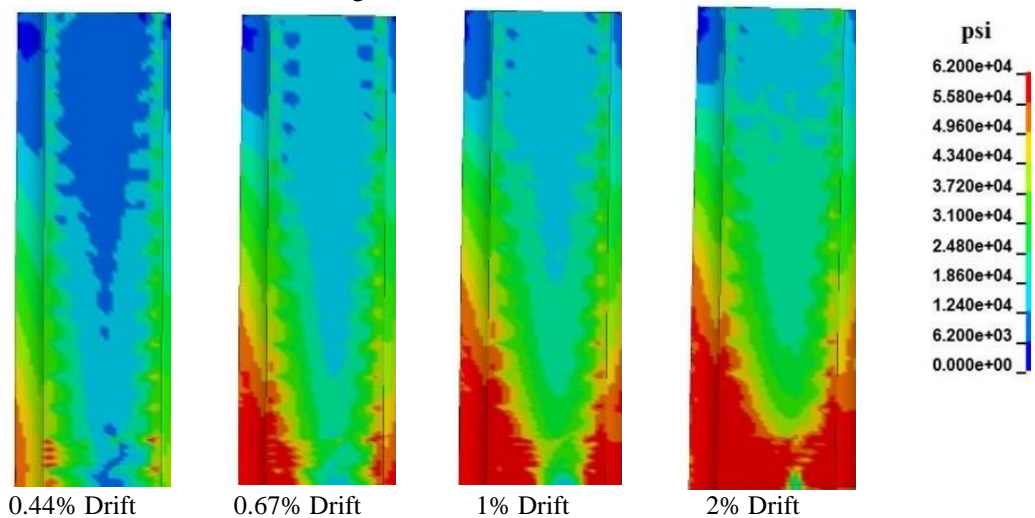


Figure 8:
Distribution of von-Mises stress contours of steel plate of Model B1

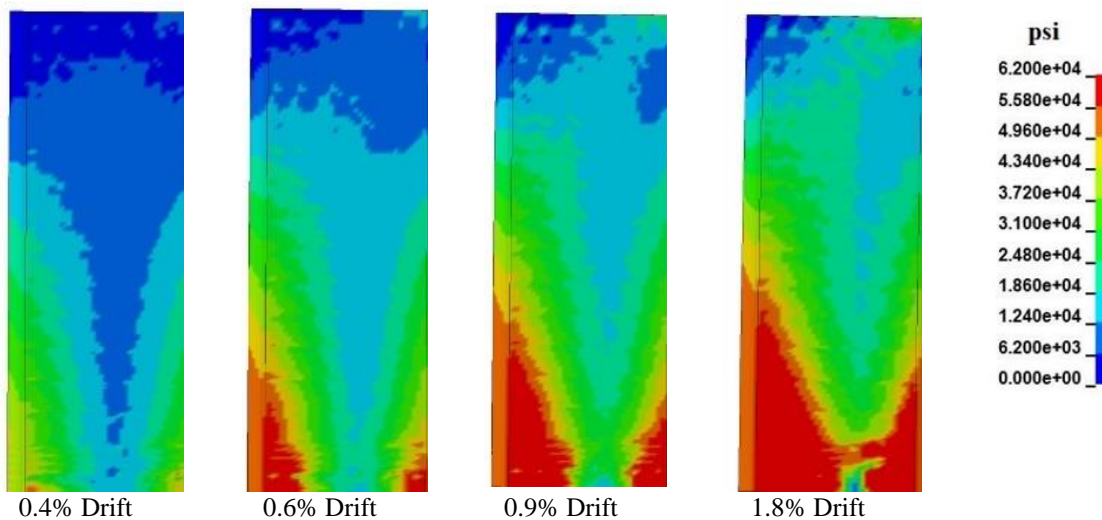


Figure 9:
Distribution of von-Mises stress contours of steel plate of Model NB1

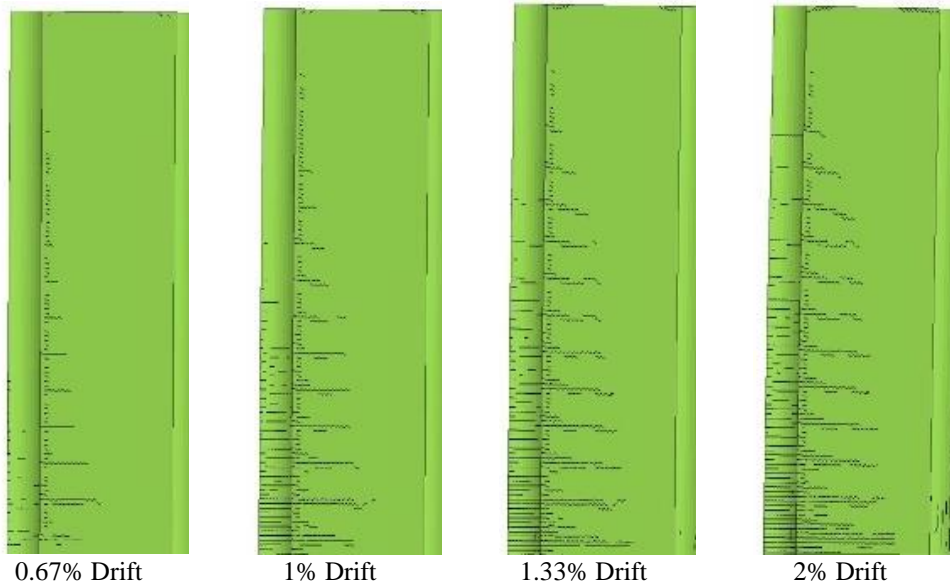


Figure 10:
Formation of concrete cracks of Model B1 under increasing wall drift

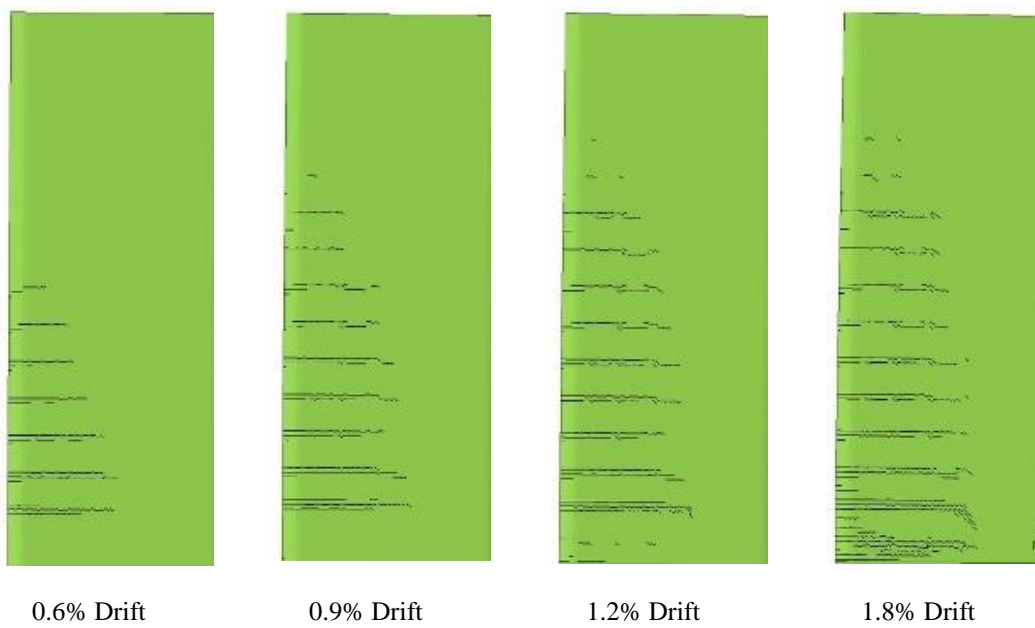


Figure 11:
Formation of concrete cracks of Model NB1 under increasing wall drift

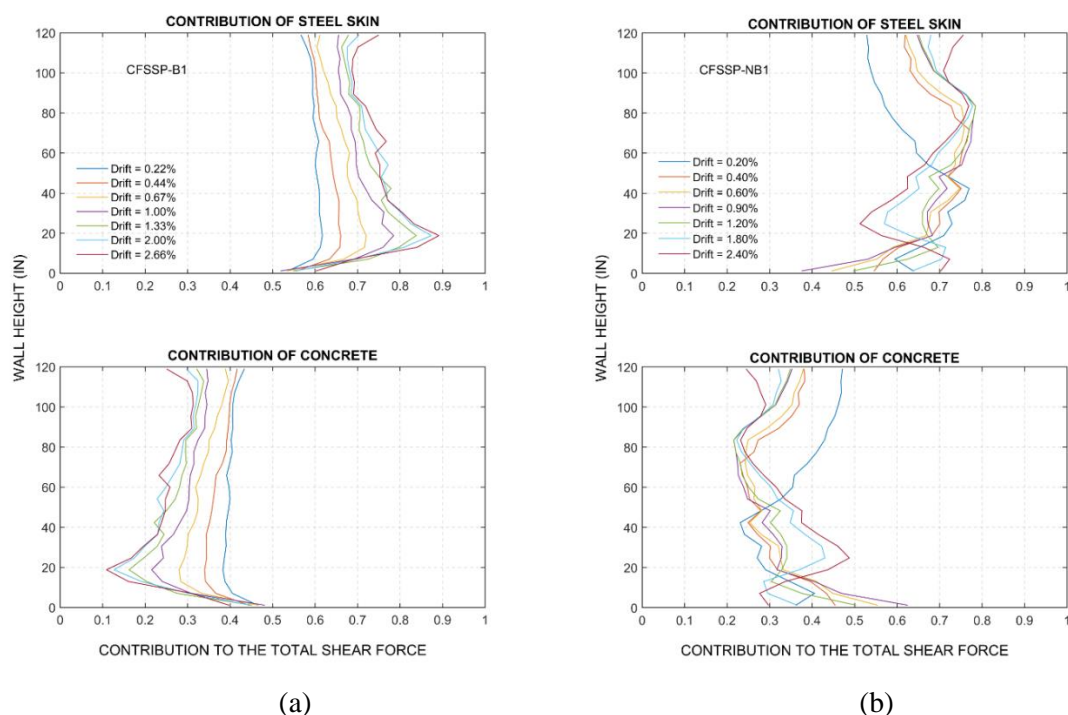


Figure 12:

Relative contribution of steel and concrete to total base shear resistance of the walls: a) Model B1, and; b) Model NB1

7. AXIAL STRESS DISTRIBUTION OF STEEL AND CONCRETE

For flexural type C-PSW/CF, the lateral force is resisted by development of plastic moment at the wall base due to bending. The plastic moment is based on the assumption that the stress distributions on the steel and concrete part of the cross-section are uniform, and taken as F_y and f'_c respectively for steel and concrete, where F_y is the yield strength of the steel skin, and f'_c is the compressive strength of the concrete. In this section, cross-section axial stress distribution, obtained from the numerical analyses, are presented. For each wall model, average axial stress histories were extracted from shell and solid elements for a certain wall elevation (specified to be 10 in.). The stresses were then plotted across the cross-section depth for specified wall drift ratio. **Figure 13** and **Figure 14** show such plots for Model B1 and NB1, respectively. The stress distributions are close the uniform stress distribution assumption shown in **Figure 1**. The plastic neutral axis locations are shown with dashed lines in the figures.

The axial stress distributions of the steel and concrete verifies the amount and significant of local plate buckling for Model NB1 which resulted in change in the relative shear contribution of steel and concrete as explained in the previous section. As seen in **Figure 14(a)** that following 1.20% drift ratio, axial stresses in the steel web plate drops significantly as a result of local plate buckling. However, such reduction in stress is not seen in **Figure 13(a)** for the steel web plate of Model B1. As explained in previous section, this behavior was related to the wall boundary elements. It was deemed that the use of full HSS had positive influence on web plate local buckling. It should be noted from the steel axial stress distribution for both models (**Figure 13(a)** and **Figure 14(a)**) that the peak stresses, on the tension side of the cross-section, reached higher values than that in the compression side. This is a result of von-Mises interaction of stresses such that, owing to hoop action due to circular shape of the boundary elements of the wall, the yield stress was increased. The opposite is true for the compression side of the cross-section (i.e., steel yield stress was reduced).

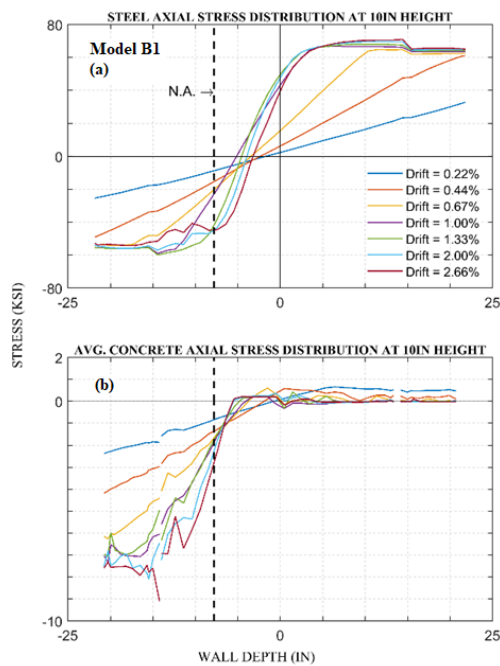


Figure 13:
Axial stress distribution of steel and concrete of Model B1 at 10in elevation

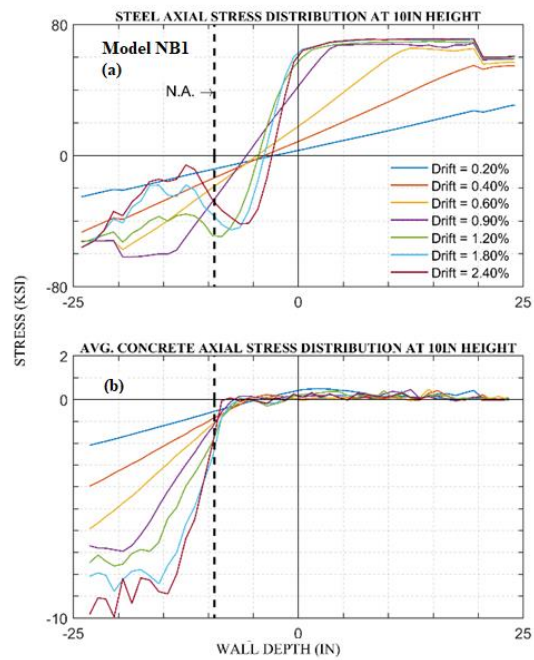


Figure 14:
Axial stress distribution of steel and concrete of Model NB1 at 10in elevation

8. CONCLUSION

In this study, two previously tested C-PSW/CF were investigated using finite element analysis. Findings from the numerical analyses are expected to extend the current knowledge on this type of walls. The findings from the study are as follows:

- Within the region of plastic hinge, steel plate attains 100% yielding only at elevations very close to wall base and at drift ratio of about 2.0%. At higher elevations within the plastic hinge, percentage of steel plate yielding is gradually reduced. Results indicated that it would be reasonable to take plastic hinge length equal to total cross-section depth of the wall.
- The von-Mises (yield) stress contours illustrated the development of wall plastic hinge with increasing drift levels. The stress contours of the steel plates, further verified the development of wall plastic hinges at about 2.0% drift ratio.
- Consistent with the flexural behavior of the walls, horizontal cracks were shown to be formed on the tension side of the wall. These cracks were shown to be increased in number and size with increasing wall drift. Moreover, it was shown that the flexural cracks were formed at locations where tie bars were used along the wall length. Compressive (vertical) cracks were shown to be formed on the outermost compression side of the wall around 2.0% drift ratio.
- It was shown that relative contribution of steel plates and concrete to total wall base shear can vary along the height of the walls with increasing drift levels. The contribution of concrete to total base shear was shown to gradually reduced with increasing wall drift (the opposite was true for the steel plates). Exception to this is when the local buckling of steel plates was significant. In this case, a shift in shear demand, from steel plate to concrete, occurred.

Axial stress distributions of steel plate and concrete were shown to be in close agreement with the uniform stress distribution assumption for calculating plastic moment capacity of the walls. Reduction in axial stress capacity at larger drifts levels was deemed to be as a consequence of local plate buckling.

REFERENCES

1. AISC (2016). "Seismic provisions for structural steel buildings." *AISC 341-16*, AISC, Chicago.
2. Alzeni, Y., and Bruneau, M. (2014). "Cyclic inelastic behavior of concrete filled sandwich panel walls subjected to in plane flexure." *Technical Rep. MCEER, 14-009*, Univ. at Buffalo, the State Univ. of New York, Buffalo, NY, MCEER.
3. Alzeni, Y., and Bruneau, M. (2017). "In-plane cyclic testing of concrete-filled sandwich steel panel walls with and without boundary elements." *Journal of Structural Engineering*, 143(9), 04017115.
4. Broadhouse, B. (1995). "The Winfrith concrete model in LS-DYNA3D." *Report: SPD/D (95)*, 363.
5. Broadhouse, B., and Neilson, A. (1987). "Modelling reinforced concrete structures in dyna3d." UKAEA Atomic Energy Establishment, Winfrith (UK). Safety and Engineering Science Div.
6. Clark, L. (1995). "CEB-FIP Model Code 1990." *Structural Engineering Review*, 1(7), 60-61.
7. Eom, T.-S., Park, H.-G., Lee, C.-H., Kim, J.-H., and Chang, I.-H. (2009). "Behavior of double skin composite wall subjected to in-plane cyclic loading." *Journal of structural engineering*, 135(10), 1239-1249.
8. Hallquist, J. O. (2006). "LS-DYNA theory manual." *Livermore software Technology corporation*, 3.
9. Hallquist, J. O. (2006). "LS-DYNA theory manual." *Livermore Software Technology Corporation*, <<http://www.dynasupport.com/manuals>>.
10. LSTC (2013). *Keyword User's Manual, Volume II, Material Models*, Livermore Software Technology Corporation (LSTC), Livermore, CA, USA.
11. Polat, E., and Bruneau, M. (2017). "Modeling cyclic inelastic in-plane flexural behavior of concrete filled sandwich steel panel walls." *Engineering Structures*, 148, 63-80.
12. Polat, E., and Bruneau, M. (2018). "Cyclic Inelastic In-plane Flexural Behavior of Concrete Filled Sandwich Steel Panel Walls with Different Cross-Section Properties." *Engineering Journal, American Institute of Steel Construction*, 55, 45-76.
13. Ramesh, S. (2013). "Behavior and design of earthquake-resistant dual-plate composite shear wall systems." PURDUE UNIVERSITY.
14. Schwer, L. "The Winfrith concrete model: beauty or beast? insights into the Winfrith concrete model." *Proc., 8th European LS-DYNA Users Conference*.
15. Wittmann, F., Rokugo, K., Brühwiler, E., Mihashi, H., and Simonin, P. (1988). "Fracture energy and strain softening of concrete as determined by means of compact tension specimens." *Materials and Structures*, 21(1), 21-32.
16. Wright, H., Oduyemi, T., and Evans, H. (1991). "The design of double skin composite elements." *Journal of Constructional Steel Research*, 19(2), 111-132.

17. Wright, H., Oduyemi, T., and Evans, H. (1991). "The experimental behaviour of double skin composite elements." *Journal of Constructional Steel Research*, 19(2), 97-110.